

Making the impulsive approximation with  $V(R) = C_n R^{-n}$ , taking the semiclassical limit  $j \rightarrow \sqrt{j(j+1)}\hbar$ , multiplying the rate constant by 2 to compensate for the even  $j$  selection rule associated with even  $l$ , and using detailed balance, we obtain

$$k_{j \rightarrow 0} \approx \frac{k_{0 \rightarrow j}}{2j+1} \approx \frac{1}{2} \frac{k_{0 \rightarrow j}}{\sqrt{j(j+1)}} \approx \frac{2\pi}{n-1} \left( \frac{C_n}{\hbar} \frac{\Gamma(1/2)\Gamma[(n-1)/2]}{\Gamma(n/2)} \right)^{2/n-1} \times v^{(n-3)/(n-1)} [j(j+1)]^{-n/(n-1)} \int_0^{w_m} dw w^{2/(n-1)} P_w(w). \quad (5)$$

For  $n=6$  and  $l=2$ , the integral is 0.9614.

The value of  $\alpha$  predicted by our model is relatively insensitive to the potential, since the exponent  $n$  determines only a small excess of  $\alpha$  [Eq. (1)] over unity. Furthermore, our model stresses the importance of the long range portion of the potential surface in rotational energy transfer which is justified by the large cross sections that have been experimentally observed. In contrast, hard ellipse models of the differential scattering cross section<sup>8,9</sup> do not yield the proper power law decrease of  $k_{j \rightarrow 0}$  with  $j$ .

We are encouraged by the agreement, shown in Table I, between calculated  $k_{j \rightarrow 0}$  and recent experimental measurements. Except for the targets He and Ne, where rotationally inelastic collisions likely reflect short range forces, the average errors are all below 30%—

which is comparable to those found in much more elaborate calculations<sup>12</sup> of RI processes.

<sup>a</sup>This work was supported by the Air Force Office of Scientific Research Grant 76-2972.

<sup>1</sup>T. Brunner, N. Smith, A. Karp, and D. E. Pritchard, *J. Chem. Phys.* **74**, 3324 (1981).

<sup>2</sup>N. Smith and D. E. Pritchard, *J. Chem. Phys.* **74**, 3939 (1981).

<sup>3</sup>A. E. DePristo, S. D. Augustin, R. Ramaswamy, and H. Rabitz, *J. Chem. Phys.* **71**, 850 (1979).

<sup>4</sup>S. Dexheimer, M. Durand, T. Brunner, and D. E. Pritchard, *J. Chem. Phys.* (submitted).

<sup>5</sup>J. Serri, A. Morales, W. Moskowitz, D. E. Pritchard, C. H. Becker, and J. L. Kinsey, *J. Chem. Phys.* **72**, 6304 (1980).

<sup>6</sup>T. Brunner and D. E. Pritchard, *Advances in Chemical Physics* (Wiley, London, 1982), Vol. 50.

<sup>7</sup>Ch. Ottinger and M. Schröder, *J. Phys. B* **13**, 4163 (1980). We assumed the polarization anisotropy for  $\text{Na}_2^*$  is the same as that for  $\text{Li}_2^*$ .

<sup>8</sup>H. J. Korsch and R. Schinke, *J. Chem. Phys.* **75**, 3850 (1981).

<sup>9</sup>M. H. Alexander and P. J. Dagdigan, *J. Chem. Phys.* **73**, 1233 (1980).

<sup>10</sup>T. Scott, N. Smith, and D. E. Pritchard, *J. Chem. Phys.* (submitted).

<sup>11</sup>Ionization potentials are from *CRC Handbook of Chemistry and Physics*, 61st ed. Additional polarizabilities from H. Margenau and N. R. Kestner, *Theory of Intermolecular Forces* (Pergamon, New York, 1971).

<sup>12</sup>P. J. Dagdigan and B. E. Wilcomb, *J. Chem. Phys.* **72**, 6462 (1980).

## A correlated walk model for thermally stimulated depolarization currents in $\alpha$ -keratin

Estela Blaisten-Barojas

*Instituto de Física, Universidad Nacional Autónoma de México, Apdo. Postal 20-364, 01000 México D. F., México*

Sérgio Mascarenhas<sup>a)</sup>

*Instituto de Física e Química de São Carlos, 13560 São Carlos, SP, Brasil*

(Received 26 October 1981; accepted 18 January 1982)

Electrical currents during the thermal heating of  $\alpha$ -keratin fibers have been reported by Menefee.<sup>1</sup> In this case the fibrous keratin constitute what is called a natural bioelectret.<sup>2</sup> This highly ordered dipolar system undergoes melting when heated, thereby inducing a depolarization current in the external circuit. The observed thermally stimulated current (TSC) shows two maxima as a function of temperature. These peaks have been attributed to the presence of two independent environments for the protein molecules in the fibrous keratin.<sup>3</sup> Recently a model has been proposed to describe the helix-coil transition of polymers<sup>4,5</sup> using correlated walks.<sup>6</sup> This approach starts with a modified Ising Hamiltonian<sup>7</sup> and includes correlation among the helical and coil states of the polymer. In this work

we show that the correlated walk model (CWM) is able to describe all the main experimental results of the TSC from  $\alpha$ -keratin fibers. Quantitative values of the parameters pertaining to the theory are also obtained from the experimental data.

Experimentally there are two TSC peaks in  $\alpha$ -keratin from highly oriented samples. These occur respectively at 487 and 507 K for porcupine quills.<sup>1,3</sup> They reverse sign when the orientation of the sample is reversed and there is no current flow if the axis of the oriented keratin is parallel to the detection electrodes. These maxima of the TSC have been interpreted as due to the existence of two distinct  $\alpha$ -helical fractions in keratin. These fractions have been experimentally confirmed by

x-ray diffraction and calorimetry.<sup>8-10</sup> We have thus applied the CWM in the following way:

(i) The polymer backbone forming helices is modeled by a polymer stretched over on a simple cubic lattice in such a way that repeated squares simulate helical turns.<sup>5</sup> Each residue is represented by a segment joining two points of this lattice. One effective hydrogen bond will be formed only when a segment completes a square with the preceding three segments, thereby giving a net oriented dipole moment. The complete helical state is attained when the polymer is wound around a single square repeatedly. The polymer will be divided in *units* of three residues. Each unit together with the last residue of the preceding unit may or may not form a square.

(ii) Two types of  $\alpha$ -helix structures will be considered in the keratin fibers. The total bond energy can be expressed as a sum of two independent Hamiltonians ( $i = 1, 2$ ):

$$H = -\frac{1}{4} \sum_{i=1}^2 K_i \sum_{\alpha=1}^{N_i} (1 + \mu_{i\alpha})(1 + \mu_{i\alpha+1}). \quad (1)$$

Here  $K_i$  represents the bond energy between two of the  $N_i$  units in the  $i$ th chain. The states of the  $\alpha$ th unit are:  $\mu_{i\alpha} = 1$  if a net oriented dipole is obtained (closed square) and  $\mu_{i\alpha} = -1$  otherwise (open figure).

(iii) The statistical weight of a given state of the  $i$ th chain of dipoles is assumed to be the product of the turn formation factor  $p_i$  if  $\mu_{i\alpha} = 1$  (or  $q_i$  if  $\mu_{i\alpha} = -1$ ) and the Boltzmann factor  $\exp(K_i/K_B T)$  if a turn follows another turn (or unity otherwise). The probabilities  $p_i$  and  $q_i$  are normalized such that  $p_i + q_i = 1$ .

For the calculation of the TSC we write the polarization  $P$  as

$$P \equiv m_0 \sum_{i=1}^2 \langle f_i \rangle = m_0 \sum_{i=1}^2 \frac{\partial \ln \lambda_i}{\partial (K_i/k_B T)}, \quad (2)$$

where  $m_0$  is the average dipole moment per turn of the  $\alpha$ -helix directed along the helix axis and  $\langle f_i \rangle$  is the ratio of the number of helical turns to the total number of units in a large portion of the protein. The functions  $\lambda_i$  are given by<sup>4,5</sup>

$$\lambda_i = \frac{1}{2} [1 + s_i + \sqrt{(1 - s_i)^2 + 4t_i}], \quad (3)$$

where  $t_i = p_i/q_i$  and  $s_i = t_i \exp(K_i/k_B T)$ . The dipolarization current is then given by

$$i = -dP/dt. \quad (4)$$

We shall also assume a linear heating rate  $b = dT/dt$  during experiments, though any variable heating rate may also be considered.

The current calculated from the CWM using Eqs. (2)–(4) can be fitted to the experimental results for  $\alpha$ -keratin from porcupine quills as obtained by Menefee.<sup>1,3</sup> Essentially the temperatures at which the TSC has maxima are related to the  $K_i$  while the peak-widths are given by the parameters  $t_i$ . The height of the peak at 507 K was fitted with experiment; this gives the number of dipoles involved in the sample used by Menefee. The

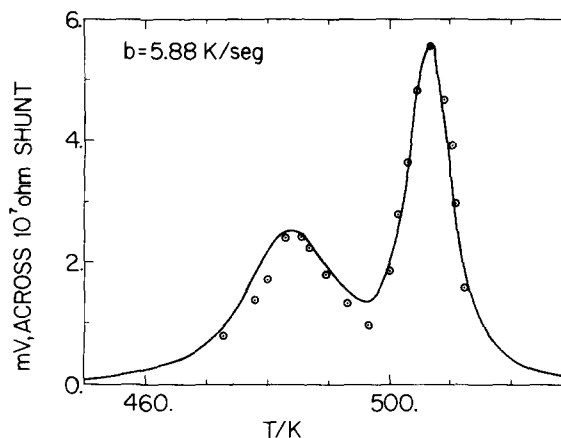


FIG. 1. Dots reproduce the voltage produced across a  $10^7 \Omega$  external shunt in a transverse section of porcupine quill, as measured by Menefee.<sup>1,3</sup> The continuous line corresponds to this calculation.

results are shown in Fig. 1 and we can conclude the following. The CWM is able to describe the TSC peaks of keratin bioelectrets and gives quantitative values of  $K_1$  and  $K_2$ , the values of hydrogen bond energies per turn of the two types of helices. It gives also  $t_1$  and  $t_2$ , the corresponding formation factors related to the entropy loss per dipole on going from a rather free configuration of a dipole in a random coil to the more ordered configuration of a dipole in a helix turn. It is very satisfactory that the values obtained here of  $K_1 = 5.21$  and  $K_2 = 6.70$  kcal/mol per turn in the helix are within the known range of hydrogen bond energies, considering that these are 3.6 residues per turn in the  $\alpha$ -helix. The values of  $t_1 = 4.5 \times 10^{-3}$  and  $t_2 = 1.3 \times 10^{-3}$  indicate that system 2 is more highly ordered than system 1. This is in agreement with the peak assignment given by Menefee.<sup>3</sup> That author identified the lower temperature peak with the less oriented fraction of  $\alpha$ -keratin characterized by fewer stabilizing cross links to the amorphous phase in the matrix. Finally it is important to point out that the relative heights of the two maxima emerging from the CWM are in excellent agreement with the experimental data.

In summary, we have shown that it is possible to extract via the CWM and TSC measurements, quantitative values of the hydrogen bond energies and order parameters of the  $\alpha$ -helix molecules encountered in keratin fibers.

One of us (S.M.), thanks the Instituto de Fisica de la UNAM for all the support it gave during his stay and especially thanks Dr. Jorge Flores for the invitation to occupy the Manuel Sandoval Vallarta visiting professor chair.

<sup>a1</sup>Manuel Sandoval Vallarta Visiting Professor at Universidad Nacional Autónoma de México.

<sup>1</sup>E. Menefee, in *Electrets*, edited by M. Perhman (Electrochemical Society, New York, 1973), p. 627.

<sup>2</sup>S. Mascarenhas, in *Topics in Applied Physics*, edited by G.

- M. Sessler (Springer, Berlin, 1979), Vol. 33, p. 321.  
<sup>3</sup>E. Menefee, *Ann. N. Y. Acad. Sci.* **238**, 53 (1974).  
<sup>4</sup>S. Fujita, E. Blaisten-Barojas, and S. Godoy, *Ferroelectrics* **30**, 299 (1980).  
<sup>5</sup>S. Fujita, E. Blaisten-Barojas, M. Torres, and S. Godoy, *J. Chem. Phys.* **75**, 3097 (1981).  
<sup>6</sup>Y. Okamura, E. Blaisten-Barojas, S. Fujita, S. Godoy, and S. Ulloa, *J. Chem. Phys.* **76**, 601 (1982).

- <sup>7</sup>S. Fujita, Y. Okamura, S. Godoy, L. García Colin, and E. Blaisten-Barojas, *Proceedings of the 8th Oaxtepec Meeting on Statistical Physics*, Jan. 1979, *Kinam A* **2**, 193 (1980).  
<sup>8</sup>E. Menefee and G. Yee, *Textile Res. J.* **35**, 801 (1965).  
<sup>9</sup>E. Menefee, *Textile Res. J.* **38**, 1149 (1968).  
<sup>10</sup>J. S. Crighton and F. Happey, *Symposium on Fibrous Proteins, Australia*, 1967, edited by W. G. Crewther (Plenum, New York, 1968), p. 409.

## Alkoxy radical radiation products<sup>a)</sup>

Harold C. Box and Edwin E. Budzinski

*Department of Biophysics, Roswell Park Memorial Institute, Buffalo, New York 14263*  
 (Received 15 December 1981; accepted 22 January 1982)

Alkoxy radicals are produced in many carbohydrate and polyhydroxy compounds<sup>1,2</sup> by exposure to ionizing radiation at low temperature. Recently, it has been recognized that ESR spectra with rather diverse hyperfine patterns can be attributed to alkoxy radicals.<sup>3</sup> In some species, so-called  $\gamma$  protons, which are three bond lengths removed from the oxygen atom (the main site of electron spin density), contribute importantly to the hyperfine pattern.

The alkoxy radicals (I) and (II) shown in Fig. 1 have been identified in irradiated ribitol and irradiated 6-methylpurine riboside (6-methyl-9- $\beta$ -D-ribofuranosyl-purine), respectively. Both exhibit strong  $\gamma$ -proton hyperfine couplings.

The  $g$  tensor and the proton coupling tensors which

describe the paramagnetic absorption of (I) and (II) as determined from ESR and ENDOR studies are listed in Tables I and II, respectively. The measurements were made on single crystals  $x$  irradiated at 4.2 K. In order to improve signal-to-noise, the helium bath was pumped during measurements to reduce the temperature to 1.5 K. Crystals of ribitol and 6-methylpurine riboside grown from aqueous solution belong to the space groups  $P2_1/c$  and  $P2_12_12_1$ , respectively, and contain four molecules per unit cell.<sup>4,5</sup>

The unpaired electron in an alkoxy radical occupies mainly an oxygen  $2p$  orbital. Maximum  $g$  value indicates the direction of the C-O bond. Thus, the oxidation sites indicated in (I) and (II) could be deduced from the  $g$  tensors by referring to the crystal structures.

TABLE I. The  $g$  tensor and proton hyperfine coupling tensors for the alkoxy radical absorption in irradiated ribitol. Principal values of coupling tensors are in MHz. Direction cosines of principal axes are with respect to the crystallographic axes  $a$ ,  $b$ , and  $c^* = a \times b$ .

Principal values	Direction cosines		
	$a$	$b$	$c^*$
$g$ tensor			
2.0459	0.940	0.179	-0.289
2.0070	-0.244	0.947	-0.206
2.0000	0.237	0.265	0.934
Hyperfine tensors			
92.54	0.501	0.833	-0.232
75.94	0.660	-0.194	0.725
73.66	0.559	-0.516	-0.648
19.12	0.456	0.860	0.227
10.70	0.785	-0.268	-0.557
-1.84	0.418	-0.433	0.798
11.46	0.748	0.054	-0.660
9.08	0.627	0.263	0.732
7.88	-0.214	0.963	-0.162

TABLE II. The  $g$  tensor and proton hyperfine coupling tensors for the alkoxy radical absorption in irradiated 6-methylpurine riboside. Principal values of coupling tensors are in MHz. Direction cosines of principal axes are with respect to crystal axes  $a$ ,  $b$ , and  $c$ .

Principal values	Direction cosines		
	$a$	$b$	$c$
$g$ tensor			
2.0391	0.116	0.613	0.780
2.0069	0.724	-0.590	0.355
2.0004	0.679	0.524	-0.513
Hyperfine tensors			
48.06	0.708	0.036	0.704
35.22	0.460	0.731	-0.501
33.14	-0.533	0.680	0.502
34.06	0.330	0.368	0.868
19.62	0.900	0.151	-0.407
11.14	-0.281	0.917	-0.281
15.52	0.017	0.973	0.226
12.88	0.507	-0.204	0.837
12.36	0.861	0.100	-0.497